REPORT DOCUMENTATION PAGE

Form Approved
OMB No. 0704-0188

1. REPORT DATE *(DD-MM-YYYY)*	2. REPORT TYPE	3. DATES COVERED *(From - To)*
04/16/2021	Final	11/17/2017-12/31/2020

4. TITLE AND SUBTITLE
Stochastic variability of fish school scattering and attenuation fluctuation effects based on collective animal behavior modeling

5a. CONTRACT NUMBER

5b. GRANT NUMBER
N62909-18-1-2016

5c. PROGRAM ELEMENT NUMBER

6. AUTHOR(S)
Christopher Feuillade

5d. PROJECT NUMBER

5e. TASK NUMBER

5f. WORK UNIT NUMBER

7. PERFORMING ORGANIZATION NAME(S) AND ADDRESS(ES)
Instituto de Física, Pontificia Universidad Católica de Chile
Avenida Vicuña Mackenna, 4860
Santiago, Chile

8. PERFORMING ORGANIZATION REPORT NUMBER

9. SPONSORING/MONITORING AGENCY NAME(S) AND ADDRESS(ES)
Office of Naval Research
Boston Regional Office
495 Summer Street
Boston, MA 02210

10. SPONSOR/MONITOR'S ACRONYM(S)

11. SPONSOR/MONITOR'S REPORT NUMBER(S)

12. DISTRIBUTION/AVAILABILITY STATEMENT
DISTRIBUTION STATEMENT A: Distribution approved for public release; distribution is unlimited.

13. SUPPLEMENTARY NOTES

14. ABSTRACT
This report contains information on the activities and accomplishments of this project.during period November 17, 2017 to December 31, 2020.

15. SUBJECT TERMS
Stochastic variability of fish school scattering and attenuation fluctuation effects based on collective animal behavior modeling

16. SECURITY CLASSIFICATION OF:			17. LIMITATION OF ABSTRACT	18. NUMBER OF PAGES	19a. NAME OF RESPONSIBLE PERSON
a. REPORT	b. ABSTRACT	c. THIS PAGE			Christopher Feuillade
					19b. TELEPHONE NUMBER *(Include area code)*
U	U	U	SAR	14	+56 9 8 766-2421

Stochastic variability of fish school scattering and attenuation fluctuation effects based on collective animal behavior modeling (Final Report April 16, 2021)

Christopher Feuillade
Pontificia Universidad Católica de Chile
Facultad de Física
Av. Vicuña Mackenna 4860
Santiago, Chile
email: chris.feuillade@gmail.com

Award Number: N62909-18-1-2016

LONG-TERM GOALS

The goal of this work is to investigate spatial and temporal fluctuations in SONAR reverberation and attenuation due to schooling fish. The purpose is to foster the improvement of propagation/reverberation codes used by the Navy, by incorporating boundary interference effects and oceanographic variability.

OBJECTIVES

The objective of this research is to develop a theory, based on a verified mathematical/computational model of acoustic scattering from multiple swim bladder fish, which includes coherent scattering and radiative interactions, and also zoologically realistic computational modeling of fish school behavior, to describe and explain stochastic variations in resonance frequency (and near resonance frequency) acoustic fish school scattering, attenuation, and target strength.

APPROACH

The personnel participating in this work at this time are: Principal Investigator: Christopher Feuillade - Ph. D. (Physics), Manchester, UK, 1977. (Visiting Professor, Pontificia Universidad Católica de Chile); Assistant: Luis Donoso - (postgraduate student, Pontificia Universidad Católica de Chile).

(1) Steady-state solution for a school: A low-frequency resonance scattering model for fish schools is used [1], which is based upon the harmonic solution of sets of coupled differential equations (the CDE model). This model uses a verified swim bladder scattering "kernel" for the individual fish [2], includes multiple scattering interactions between the fish, and calculates the aggregate scattering field by coherent summation.

The behavior of a whole school is represented by the following set of coupled second-order differential equations:

$$\begin{aligned} m_1\ddot{v}_1 + b_1\dot{v}_1 + \kappa_1 v_1 &= -P_1 e^{i(\omega t+\phi_1)} - \sum_{j\neq 1}^{N} \frac{\rho e^{-ikr_{j1}}}{4\pi r_{j1}} \ddot{v}_j \quad ; \\ &\cdots \\ m_n\ddot{v}_n + b_n\dot{v}_n + \kappa_n v_n &= -P_n e^{i(\omega t+\phi_n)} - \sum_{j\neq n}^{N} \frac{\rho e^{-ikr_{jn}}}{4\pi r_{jn}} \ddot{v}_j \quad ; \\ &\cdots \\ m_N\ddot{v}_N + b_N\dot{v}_N + \kappa_N v_N &= -P_N e^{i(\omega t+\phi_N)} - \sum_{j=1}^{N-1} \frac{\rho e^{-ikr_{jN}}}{4\pi r_{jN}} \ddot{v}_j \quad . \end{aligned} \tag{1}$$

where P_n and ϕ_n are the amplitude and phase of the external field incident on the n-th swim bladder, and r_{jn} is the distance between the j-th and n-th swim bladder, etc. The quantities m_n, b_n, κ_n, etc. allow for different values for the swim bladder radii, damping, etc., to be incorporated to represent a diverse range of individual fish properties within the school. Every swim bladder is driven both by the external field and the scattered fields from the other swim bladders.

Steady state solutions are obtained by substituting $v_1 = \overline{v}_1 e^{i\omega t}, v_2 = \overline{v}_2 e^{i\omega t}, \ldots$ etc., in (1), leading to a matrix equation $\mathbf{Mv} = \mathbf{p}$, where $\mathbf{v} = \{\overline{v}_1, \ldots, \overline{v}_n, \ldots, \overline{v}_N\}$ and $\mathbf{p} = \{-p_1 e^{i\phi_1}, \ldots, -p_n e^{i\phi_n}, \ldots, -p_N e^{i\phi_N}\}$ contain the steady-state harmonic volume oscillation amplitudes and external fields, respectively, for the individual bladders, and $\mathbf{M}$ is an $N \times N$ matrix with elements:

$$M_{nn} = \kappa_n - \omega^2 m_n + i\omega b_n \quad ; \quad M_{nj} = \frac{-\omega^2 \rho e^{-ikr_{jn}}}{4\pi r_{jn}} \quad (n \neq j) \quad . \tag{2}$$

Each diagonal term [i.e., $M_{jj}\,(j = 1, \ldots, N)$] describes the uncoupled resonance behavior of an individual bladder, including variations in size, damping, depth etc. The off-diagonal elements [i.e., $M_{nj}\,(n, j = 1, \ldots, N;\, n \neq j)$] describe the radiative coupling between the bladders. The solution $\mathbf{v} = \mathbf{M}^{-1}\mathbf{p}$ describes steady-state scattering from the whole school as a function of the external field amplitude and frequency. From the $\overline{v}_n$, the target strength (TS) is then calculated as:

$$TS = 10\log_{10}\left[\frac{\omega^4\rho^2 \mid \sum_{n=1}^{N} \overline{v}_n e^{-ikr_n} \mid^2}{(4\pi)^2 P^2}\right] , \tag{3}$$

where $P_1 = P_2 = \cdots = P_N = P$. Since both multiple scattering and coherent addition of the scattered fields are included, the ensemble scattering shows the effects of radiative coupling between fish, and also constructive and destructive interference leading to Bragg scattering effects.

(2) Dynamic school behavioral model: In order to incorporate acoustic interactions realistically, the relative locations of the individual fish within the school are required as an input. To provide a description of fluctuating levels of scattering from schools, a self organizing model of school formation in three-dimensional space has been developed [3], based on biological principles of collective animal behavior [4].

There are two main rules for describing the collective behavior, which is a function of alignment and repulsive and attractive tendencies affecting the position and orientation of the individual fish. First, the

fish seek to maintain a minimum distance between themselves and their nearest neighbors to avoid collisions [5]. Second, if the fish are not performing an evasive maneuver, they seek to maintain their mutual alignment, to prevent the ensemble from dividing and separating [3,4]. Taking these two rules into account, it is possible to predict and calculate the direction of each fish as a function of time, and the evolution of the entire ensemble configuration may thereby be determined.

A computer model has been developed incorporating these behavioral principles, which predicts the time evolution of all the individuals within a school of any given number of fish, and thus gives a realistic zoological description of the motion of the whole ensemble. The behavior to which the school evolves has been found to depend on the initial constraint values [3]. An evolution into a cylindrical form is shown in Fig. 1, which has been the primary behavior type on which the research has concentrated over the period of this report.

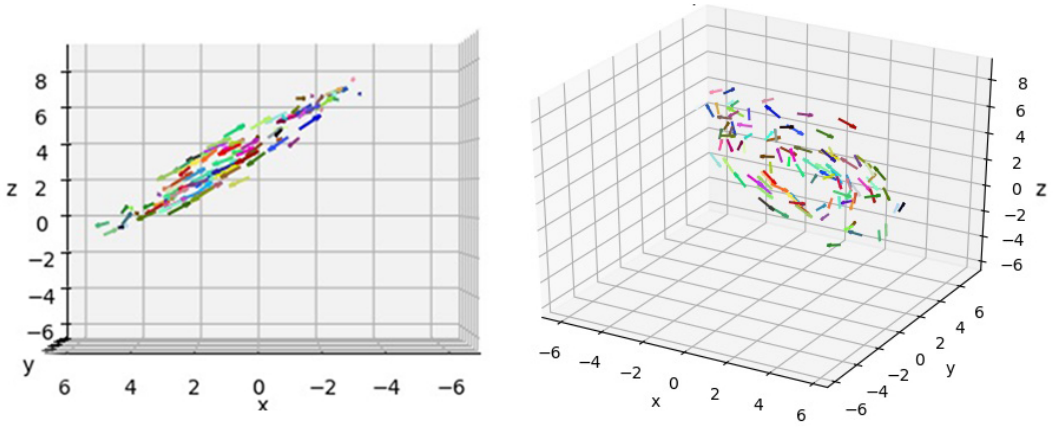

Figure 1: Locations of individual fish in a disk-shaped school. The dynamic fish school model has been used to generate the time evolution of an ensemble of 100 ***fish into a discoid form. The two figures depict the geometrical positions of the fish at the same instant of time, but from different viewing angles.***

(3) T-matrix approach for scattering from cylindrically shaped schools: To describe low-frequency acoustical scattering from schools, considered as a single "effective medium" (EM) object, a T-matrix method has been used to represent the schools [6]. The incident field is described by

$$\phi_o(\mathbf{r}) = \sum_n a_n Re\psi_n(\mathbf{r}) \ , \tag{4}$$

and the scattered field by

$$\phi_s(\mathbf{r}) = \sum_n f_n \psi_n(\mathbf{r}) \ , \tag{5}$$

where $Re\psi_n(\mathbf{r})$ and $\psi_n(\mathbf{r})$ are the regular and outgoing partial wave solutions of the wave equation used to expand the field. The scattered field is determined by solving the matrix equation

$$\mathbf{f} = -\mathbf{ReQQ}^{-1} = \mathbf{Ta} \quad \Longrightarrow \quad \mathbf{T} = -\mathbf{ReQQ}^{-1}, \tag{6}$$

where $\mathbf{T}$ is the T-matrix for the school scatterer, which relates the incident, and scattered, field expansion coefficients, a_n, and f_n, respectively.

The elements of the matrix $\mathbf{Q}$ are obtained by integrating over the surface of the object, which, for cylindrically shaped schools, is represented by using a "superspheroid", which is a 3-D object generated

by using the equation for a "super-ellipse" [i.e, $(x/a)^s + (z/b)^s = 1$, where $s = 2n, n = 1,2,3,\ldots$], and revolving around the axis of symmetry [7]. For $s = 2$, the object is a simple spheroid with aspect ratio $\alpha = b/a$. As s increases, the shape of the object approaches a right circular cylinder of diameter $2a$ and length $2b$.

The internal acoustical properties of the EM school scatterer are described by an effective wave number k_e, which is dominated by the collective action of resonance scattering from the swim bladders. In the case where the swim bladders are identical, this is given by

$$k_e^2 = k^2 + 4\pi n\mathbf{S} \tag{7}$$

where n is the density of fish (and, therefore, of swim bladders) per unit volume, k is the propagation wave number for water (without fish), and $\mathbf{S}$ is the scattering amplitude of a single swim bladder [8].

RESULTS

(a) Time-evolution of schools into discoid forms

Using the dynamic school model, the behaviors to which fish schools evolve as a function of time has been found to depend on the initial constraint values. These specify the maximum and minimum distances from its nearest neighbors within the school that each fish will try to maintain. This may depend, for example, on the presence or absence of predators, as well as other environmental factors.

Figure 1 shows the instantaneous positions of 100 fish in a school, where the initial constraints have been chosen so that the form of the school evolves into a disk. Once the discoid shape is attained, the fish continue to revolve around the axis of the disk, maintaining the same overall configuration, although the radial positions of individual fish vary, as well as their relative positions with respect to each other. The axis of rotation of the overall discoid school also varies widely in both angle and location, as time passes.

(b) Analysis using a right circular cylinder paradigm

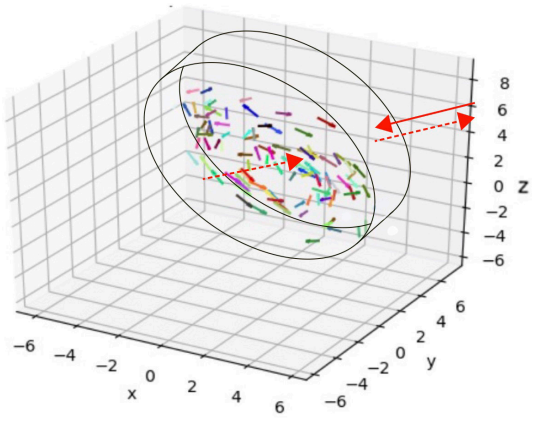

Figure 2: Cylinder paradigm for discoid schools. The school on the RHS of Fig. 1 is approximated as a cylindrical object. The solid red arrow indicates the incident field, and the dashed lines indicate reflections from the front and rear surfaces of the cylinder. Other directions of incidence are possible.

As a first step towards characterizing scattering from discoid schools, the school may be visualized and approximated as a single cylindrical object, as depicted in Fig. 2. At low frequencies, the variation of

the scattering, and therefore target strength, is determined by the size and properties of the cylinder, which is assumed to have the average dimensions of the fish school medium, (i.e., the closed volume of water containing the fish school).

Observation of the evolution of the school example shown in Fig. 1, over many time steps, indicates that the cylindrical form which circumscribes the school, in this case, has a radius of about 3.5-5m, and an axial width of about 0.5-1m.

(c) Computation of scattering from discoid schools

Figure 3 shows the results of CDE scattering computations performed for cylindrical schools, as depicted in Fig. 2, of axial width 1m, and radius: 3m, 4m, 5m and 6m. The number of fish is kept at 297 for all of these cases. To facilitate these computations, the cylindrical schools were packed using a random algorithm, rather than the dynamic model. The target strength shown is, in each case, an average over 20 random configurations of the fish locations. The angle of incidence, in every case, is 90 deg to the axis of rotation of the schools. In these examples, the individual fish have resonance frequencies around 480 Hz, and this is reflected in the overall target strength distributions shown in the figure. In order to emphasize the resonance effects on the ensemble behavior, multiple scattering processes (which tend to suppress the ensemble resonance) are not included for this computation.

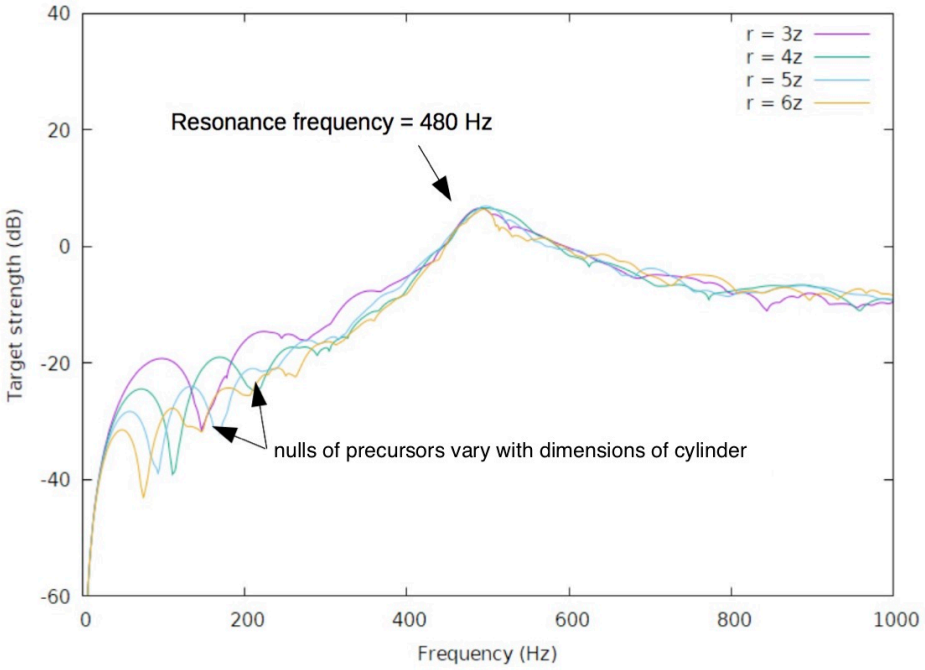

Figure 3: Target strength of schools of varying cylindrical radius. Computations are performed for cylindrical schools, as depicted in Fig. 2, of axial width $z = 1$m, and radius: $r = 3$m, 4m, 5m and 6m. The positions of the nulls of the precursors vary as the radius of the cylinder is increased.

For individual ensemble configurations of fish locations, Bragg scattering interference effects cause wide variations in the target strength as the frequency changes. [Note: This is not shown here, but is treated at greater length as part of the discussion of Fig. 9.] The averaging over 20 random configurations removes many of the Bragg scattering interference variations but, at low frequencies, below the resonance region, a number of persistent oscillatory features (which we term “precursors”)

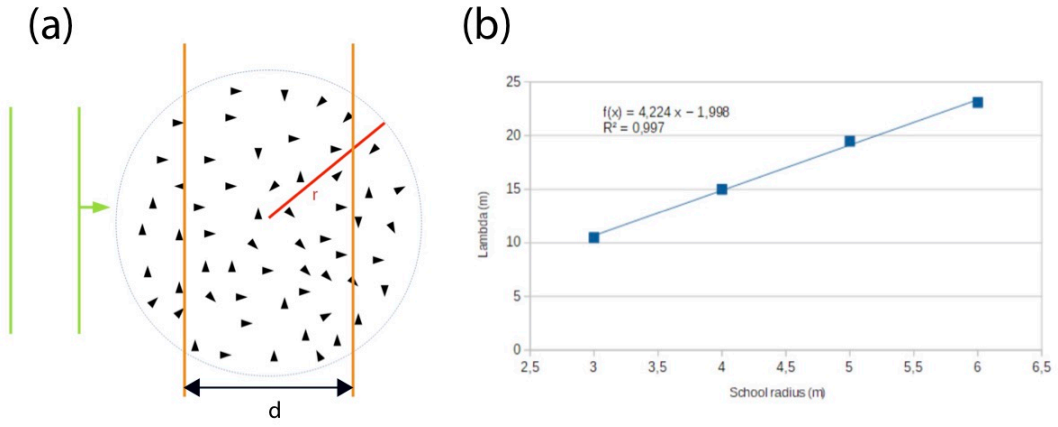

Figure 4: Scattering analysis using "two planes." (a) Back scattering of an incident plane wave is analyzed using two parallel planes, normal to the direction of incidence, and distance d apart, cutting through the cylindrical school [view from top]. (b) Reflections from the planes interfere and lead to frequency variations due to Bragg scattering (i.e., the precursors seen in Fig. 3). The wavelengths λ at which nulls occur are linearly dependent on the cylindrical radius.

are seen. These are Bragg scattering variations due to frequency dependent interactions between reflections from the front and rear curved surfaces of the cylinder (see Fig. 2), and depend on the overall dimensions of the school. It may be seen in Fig. 3 that the nulls of the precursors move progressively lower in frequency as the radius of the cylindrical schools is increased.

A simple interpretation of this phenomenon can be obtained by representing the overall scattering from the school using two parallel planes, as shown in Fig. 4(a) [9]. Reflections occur at both of these two planes, which leads to variations in the back scattering amplitude (and target strength) as a function of frequency, due to Bragg scattering. These are manifested as the lowest frequency, or first, precursors seen in Fig. 3. The wavelengths corresponding to the frequencies at which the nulls of these precursors occur are plotted against the radius of the cylindrical schools in Fig. 4(b). In the case of Fig. 3, there is a direct linear relationship between the first precursor minimum and the radius of the cylindrical school.

(d) Effect of multiple scattering on the target strength

The target strength variations seen in Fig. 3 do not include the effects of multiple scattering between the fish swim bladders. Figure 5 shows the variation of target strength for a cylindrical school of axial width 1m, radius 3m, and 675 fish, for computations where multiple scattering interactions both are, and are not, included. The curves are the result of averaging over 20 random school configurations, and the fish locations are the same for both sets of randomizations. The angle of incidence is again 90 deg to the axis of rotation of the schools. Here, the resonance frequency of an individual fish is close to 1 kHz, and the calculation extends over a frequency range of $0 - 5$ kHz.

Figure 5 indicates that multiple scattering reduces the ensemble target strength in the resonance region, but the two curves are essentially identical elsewhere. Some Bragg scattering variations are seen above the resonance frequency. These are still evident after averaging over 20 configurations, but will be largely removed when averaging over a much larger number of configurations. The low frequency precursors are not affected by multiple scattering, and are not removed by averaging.

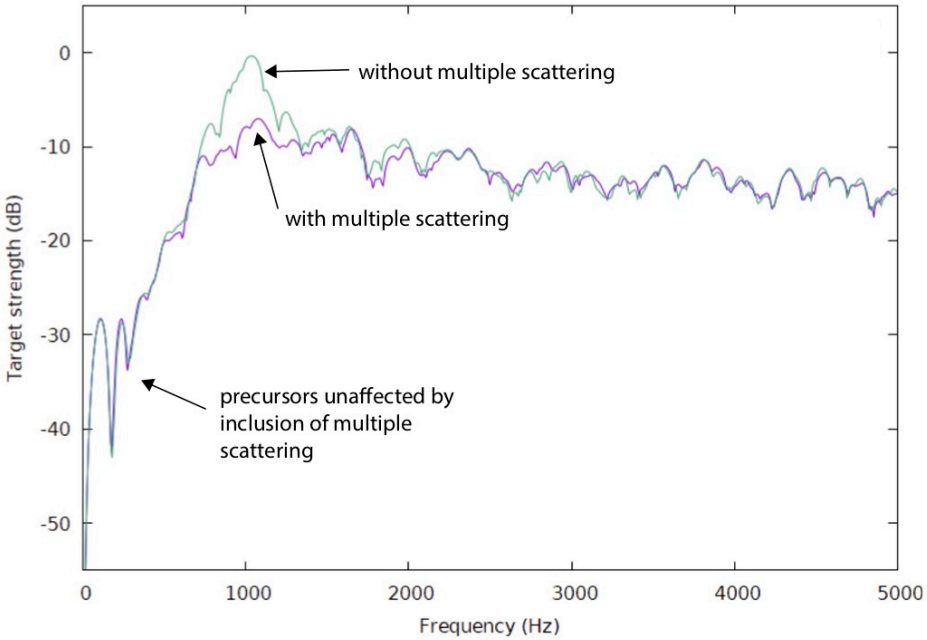

Figure 5: Effect of including multiple scattering. Target strength variations are shown for a cylindrical school of 675 ***fish, both with and without inclusion of multiple scattering effects between the fish. Both curves are the result of averaging over 20 time intervals.***

(e) Determination of school dimensions using low-frequency scattering variations

Figure 6 shows the results of computing the TS of the dynamic time-evolving school of Fig. 1 using the CDE method. The curves show the TS variation for ensonification parallel to an estimated mean axis of rotation of the fish school (the actual axis of rotation at any point in time varies widely), and also perpendicular to this mean axis. The TS curves are the average of 21 sequential time points for the two ensonifications. The first precursors indicated in Fig. 6 may be used to estimate the radius of the school from these curves, using the two planes approach outlined in Fig. 4. For ensonification parallel to the mean axis of symmetry, and using Fig. 4(b), the frequency of the first precursor corresponds to a school radius $\approx$ 3.4 m. Similarly, for ensonification perpendicular to the mean axis, the frequency of the first precursor indicates a school radius $\approx$ 4.5 m. These results compare well with the approximate estimates of the range of radial values seen in the visualizations produced by the dynamical model, from which the frame shown in Fig. 1 is taken.

Further calculations (not included here), made on schools of spherical form, have also been analyzed using an analogous two-planes approach, and show similar results. The overall conclusion is that, at low frequencies, the average acoustic scattering is predominantly determined by the geometrical form of the entire school, rather than the behavior, or interactions, of individual fish.

(f) The T-matrix approach

The previous examples discussed indicate that, at sufficiently low ensonification frequencies, fish schools scatter as a single object. Figure 6 also depicts a vertical dashed line. The position of this line indicates the frequency for which $\lambda/s = 4$, where s is the average spacing between neighboring fish in the school. This frequency (in this case, 517 Hz) is the approximate theoretical upper limit frequency for the EM assumption to be applicable [8]. This assumption assumes that the fish school is a single

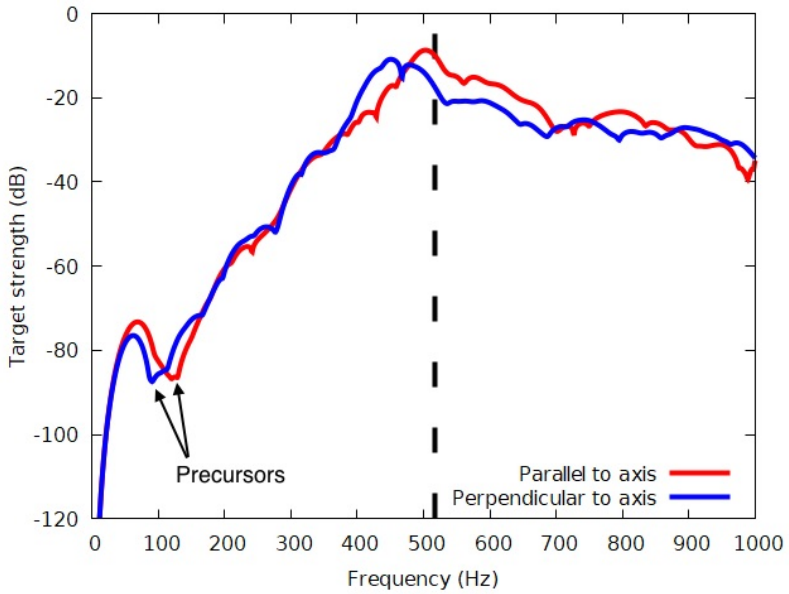

Figure 6: Averaged target strength frequency distributions for the school of 100 fish shown in Fig. 1. The fish assumed a discoid rotational configuration which could be modeled as a cylinder, and the dimensions of the school estimated from the frequency positions of the "precursors," as indicated. The averages were taken over 21 different time points of the fish school motion. The vertical dashed line represents the frequency where $\lambda/s = 4$, and is the approximate high-frequency limit (in this case, 517 ***Hz) for application of an EM assumption, where the school is treated as a single object.***

medium with acoustic properties described by Eq. (7), i.e., that the medium depends acoustically on the collective properties of the constituent fish scatterers within it. Above this frequency limit, the assumption progressively ceases to apply, because the frequency eventually becomes high enough for the acoustic field to begin to resolve and interact with the fish as individuals, and the school no longer responds as a single scatterer. Note that the scattering analysis using the precursors, shown in Fig. 6 for the school of Fig. 1, has concentrated on frequencies below this limit.

To study this further, a computer code was developed which implements a T-matrix method to predict scattering from a cylindrical school, representing the cylinder as a superspheroid [7]. Figure 7 shows a comparison of TS predicted using this T-matrix approach, assuming the fish school is a single scattering object, with that obtained using CDE. The school has a radius of 3m and a width of 1m, and contains 297 fish. The resonance frequency of an individual fish is 894 Hz. The angle of incidence is 90 deg to the axis of symmetry. The school used for the CDE analysis is packed using a random algorithm. The acoustic properties of the school used in the T-matrix analysis are given by Eq. (7), using the equivalent packing density. Again, the vertical line indicates the frequency limit for application of the EM assumption, which in this case is 1381 Hz. It is seen that, up to about 1 kHz, there is good agreement between CDE and the T-matrix method, further confirming the low frequency geometrical scattering properties of fish schools. Above 1 kHz, the curves begin to diverge. Above the EM frequency limit the two methods differ markedly, and the T-matrix analysis predicts typically lower values of TS than CDE, which has also been seen in previous studies [8].

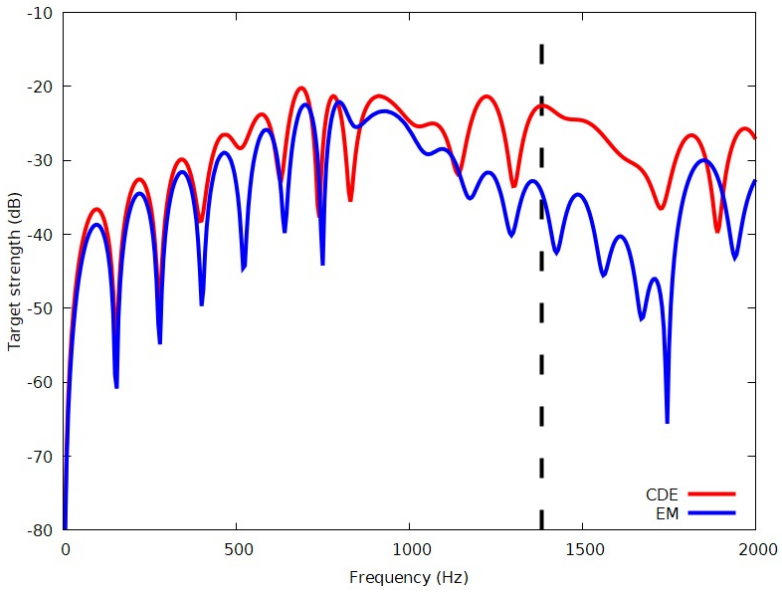

Figure 7: Comparison of the frequency variation of the target strength between the T-matrix method and the CDE method. The vertical dashed line shows the approximate high frequency limit at which the EM assumption is valid (in this case, 1381 ***Hz). Note that in the low frequency region, up to about*** 1 ***kHz, there is good agreement between the two modeling approaches.***

(g) Averaged low-frequency geometric scattering from fish schools

Figure 8 shows the results of computing the TS of the time-evolving school of Fig. 1 using both the CDE method and the T-matrix method. The resonance frequency of an individual fish for this example is now taken to be 894 Hz. The blue curve shows the TS variation, calculated using CDE, for ensonification from a direction along the axis of symmetry of the school, where it is assumed that the fish school takes the form of a cylinder with radius 4.5 m and width 0.5 m, and that the fish are randomly located within this cylinder. While the exact fish locations for each randomization are different, the average fish density throughout the school is uniform. The blue curve shows an average over 50 randomizations of the locations of the 100 fish. The average is taken over the values of the bracket [...] in Eqn. (3), before the logarithm is evaluated. The curve indicates a maximum value of the school TS of about 5 dB, at a frequency close to the individual fish resonance frequency. The predicted TS also shows a dip at about 1500 Hz. This is due to Bragg scattering interference between the signals reflected at the front and rear flat surfaces of the cylinder. Since it is assumed that the speed of sound in sea-water is $c = 1500$ m/s, then at a frequency of 1500 Hz, the wavelength is 1 m, which is twice the nominal distance between these two flat surfaces.

The black curve shows the corresponding variation of TS obtained by treating the ensemble as a single EM scattering object using the T-matrix method. Again, it is assumed that the school contains 100 fish contained within a cylindrical form with the same dimensions, and uses a collective medium propagation speed given by the Eqn. (7). A peak in TS is also seen around 894 Hz, but with a maximum value a few dB less than that predicted using CDE. Also, a much more pronounced dip in TS is seen at about 1500 Hz, again due to Bragg scattering interference. Since the boundary between the interior medium of the school and the water is exactly demarcated when making the EM assumption and using a T-matrix computation, a much deeper interference minimum is observed.

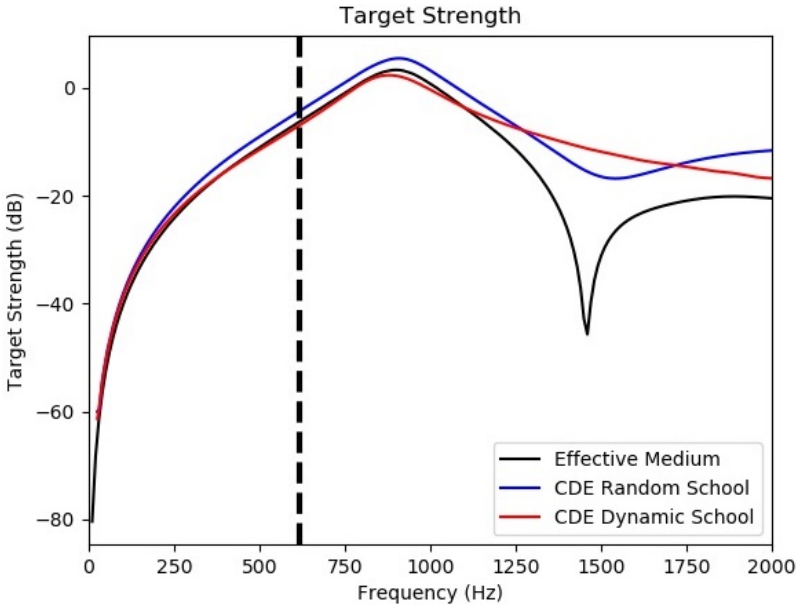

Figure 8: Target strength variations for the school of 100 fish shown in Fig. 1. Red curve: CDE target strength averaged over 50 time points of fish school motion predicted by the dynamic model. Blue curve: CDE target strength averaged over 50 randomly populated schools of the same cylindrical form and dimensions. Black curve: target strength computed using the T-matrix method, treating the school as a single cylinder. The vertical dashed line shows the approximate high frequency limit at which the EM assumption is valid (in this case, 618 ***Hz).***

The red curve is also a TS variation produced using CDE, but is the result of averaging over 50 time points of the evolution of the school motion of 100 fish, produced using the dynamic fish school model. Again, the peak is seen at about 894 Hz, and has approximately the same maximum value as the other two models. However, in this case, the Bragg scattering interference dip at 1500 Hz is not observed. The reason for this may be discerned by looking at a still from an animation from the dynamic model, as shown in Fig. 1. While the fish ensemble clearly maintains a cylindrical pattern overall, the variation of the locations of fish within the school, and especially at the edges of the school, is looser and statistically distinct from that predicted by applying a random location approach (as used above to produce the blue curve). Also, the average fish density in the school is not uniform, and varies with both position and time. Because of the looser variation in the fish locations, the edge of the school is less well-defined, so that the interference minimum between reflections from the front and rear faces of the school is not generated.

The vertical dashed line in Fig. 8 indicates the frequency, in this case 618 Hz, for which $\lambda/s = 4$, i.e., the upper limit frequency for applying the EM assumption in this case [8]. It may be seen here that Fig. 8 indicates good agreement with the CDE results for both the randomized school and the dynamic school up to a frequency of about 1100 Hz, where it begins to deviate significantly from them.

(h) Statistical variations in geometrical scattering from schools

Figure 9 shows further details of the averaging procedure that was used to produce the blue and red curves of Fig. 8. The fine curves in Fig. 9(a) show the variation in TS for 50 individual random configurations of fish positions within the school. The broad curve shows the average TS for the randomized school, and is identical to the blue curve in Fig. 8. It may be seen, below about 750 Hz, that the fine curves deviate little from the average curve, indicating that, at these lower frequencies, the individual TS variations are almost identical. This indicates that the acoustic wavelength here is sufficiently long that variations in the fish locations within the different randomized ensembles will not give rise to significant changes in the phase sum $\left| \sum_{n=1}^{N} \bar{v}_n e^{-ikr_n} \right|$ appearing in Eq. (3). However, above 750 Hz, this condition gradually ceases to apply, and the individual TS variations increasingly begin to differ from each other and from the average curve. Nevertheless, note also that a prominent feature of most of these curves is that they show Bragg interference minima, typically between about 1400 Hz and 1800 Hz. This suggests that, while the individual randomizations differ in their detailed configuration of fish locations, the uniformity of the fish density ensures that they generally still give rise to a definite boundary between the fish school ensemble and the external water, enabling Bragg interference to occur.

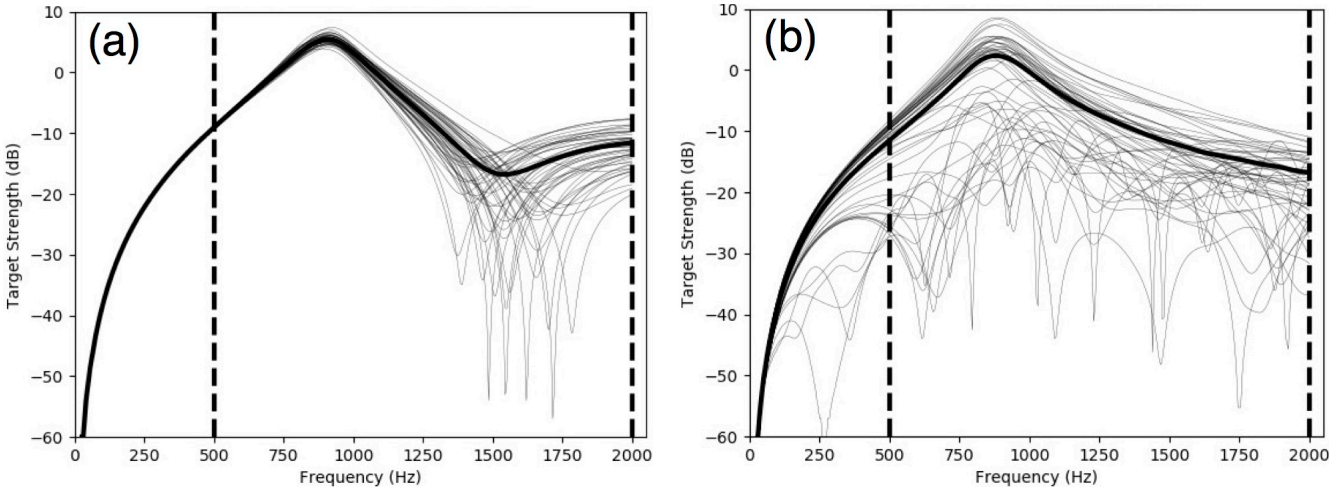

Figure 9: TS of schools with variable distributions of fish. (a): Random school. Broad curve: average TS of 50 randomized configurations of 100 ***fish. Fine curves: TS of individual configurations. (b): Dynamic school. Broad curve: average TS of*** 50 ***time points of a dynamic school of*** 100 ***fish. Fine curves: TS distributions for individual time points. Vertical dashed lines: frequencies where histograms were obtained, i.e.,*** 500 ***Hz and*** 2000 ***Hz.***

Figure 9(b) shows the corresponding individual and average TS curves obtained using 50 time points from the dynamic school model. The broad curve is equivalent to the red curve in Fig. 8. What is immediately noticeable here is that the individual TS curves deviate from the average curve practically throughout the entire frequency range displayed. Contrasting Figs. 9(a) and 9(b) shows that there is a significant difference in the statistical characteristics of the scattering from the two types of school. Unlike the random school, there is evidence of large phase cancellation effects in the dynamic school case, even at frequencies below 750 Hz. The reason for this may be observed in the single animation frame depicted in Fig. 1. The density of fish within schools generated by the dynamic model is typically non-uniform, so that the distances between neighboring fish are highly variable, and phase interactions of the scattered fields from different fish can lead to strong interference effects, and result in significant

variations in the TS distribution, over a wide range of frequencies. These variations are completely different for each configuration of fish locations. The dynamic model is based upon natural observations of fish school behavior, and so the type of variations observed here probably represent a better stochastic representation of real fish school scattering fluctuations.

A better appreciation of the difference in the statistical characteristics of scattering from the two types of school may be obtained from Figs. 10(a) and 10(b). The two vertical dashed lines in Figs. 9(a) and 9(b) indicate frequencies (i.e., 500 Hz and 2000 Hz) at which the back scattered intensity from $10,000$ configurations of schools of each type were accumulated into datasets, and used to produce histograms showing the intensity distribution. The intensity was determined by evaluating the bracket [...] in Eqn. (3) for each configuration, at the two frequencies. Figure 10(a) shows the intensity distribution for the two types of schools at 500 Hz. The orange curve applies to the random schools. Note that the dataset has a predominantly narrow unimodal and symmetric distribution. This reflects the fact that, as seen from Fig. 9a, at frequencies below 750 Hz, the scattering shows little variation between the individual configurations of the random school. The blue curve shows the corresponding data for the dynamic school. In contrast to the previous case, this dataset is apparently bimodal, with one intensity peak close to that for the random school case, and another peak close to zero intensity, and it varies over a much wider range of values. This histogram mirrors the behavior seen at 500 Hz in Fig. 9(b), with wide variations in scattering at the lower frequencies.

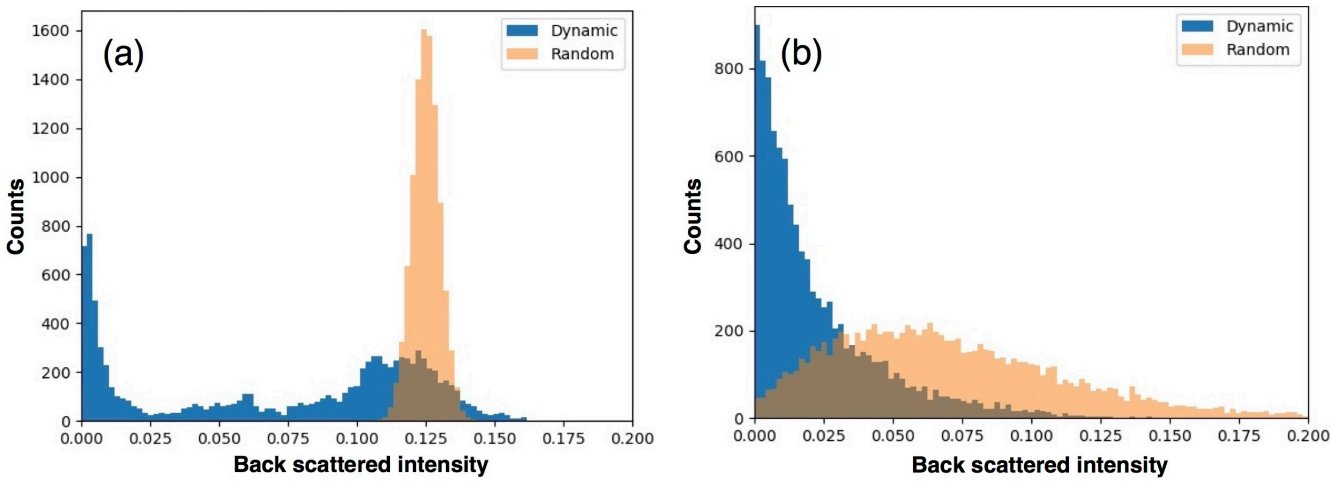

Figure 10: Back scattered intensity of schools of fish. All histograms represent datasets of $10,000$ ***total points. Orange: intensity distributions for the random schools shown in Fig. 9(a). Blue: intensity distributions for the dynamic schools shown in Fig. 9(b). (a):*** 500 ***Hz. (b):*** 2000 ***Hz.***

Figure 10(b) shows the corresponding datasets at 2000 Hz. This time, for the randomized school case, the histogram indicates a broad right-skewed unimodal distribution, reflecting the more disperse distribution of TS values seen in Fig. 9(a) at 2000 Hz. The distribution for the dynamic school at 2000 Hz shows a strongly right-skewed unimodal distribution with a lower bound very close to zero. Overall, it may be seen that, while the average TS distribution for the two types of school are very similar, as shown by comparing Figs. 9(a) and 9(b), the underlying statistical variations for the two cases are distinctly different.

CONCLUSIONS

In this work, computer simulations have been used to implement a coupled differential equation (CDE) fish school scattering model, together with a biologically based dynamic school behavioral model, to study frequency variations of low frequency acoustic scattering from schools of swim bladder fish. In particular, analysis has been performed on ensemble scattering behavior which results from dynamically generated schools of discoid form, where inputs to the dynamic school behavioral model were chosen which cause the fish schools to rotate like a disk around a central axis. The scattering from these objects has then been analyzed using a thin right circular cylinder paradigm, to investigate the characteristic ensemble target strength (TS) values and variations, as a function of frequency, of these objects.

Analysis of the cylindrically formed schools using a "two-planes" approach shows that, at low frequencies, the school behaves acoustically, on average, like a single object, so that the frequency variations of the TS are determined by the geometrical shape of the school. This geometrical scattering phenomenon has been further investigated by using an effective medium assumption to describe the propagational characteristics within a fish school, which is then coupled with a T-matrix method to describe the scattering from schools which attain cylindrical form. This shows good agreement with calculations obtained for the same type of schools using the CDE model, at frequencies where the effective medium assumption is applicable.

Analysis of the acoustic scattering from schools generated using the dynamic school model, together with analysis of scattering from schools of the same shape and dimensions, but randomly populated, using the CDE approach, confirms that, at low frequencies, both types of schools behave acoustically like a single object, and that the average frequency variations of TS are predominantly determined by the geometrical shape of the school in both cases. This observation, and the close correspondence between the variations of TS predicted using the CDE method, for both the dynamically evolved fish schools and for randomly generated schools, is based upon averaging of the scattering from the schools over many configurations of the fish locations within them. For any one particular configuration, the variation of the TS may deviate markedly from the average behavior. The CDE approach has been used to investigate this aspect of the problem, by analyzing fluctuations in scattering from schools as the configuration of fish within them varies.

The research has shown that fluctuations in TS from biologically based schools, and those from randomly generated schools, show different statistical characteristics. The physical reason is that for randomly generated fish schools, while the fish positions vary for each configuration, the overall fish density remains uniform throughout the ensemble. However, it is clear, from animations of fish school motion produced using the dynamic model, that this is not true for real fish schools. These show very uneven fish density, with much looser and ragged associations of fish. Comparisons of histograms for the back scattered intensity from the two types of schools show completely distinct types of datasets. This suggests that the fluctuation characteristics of fish schools in the sea may be usable to design a statistical classifier, which could be used to separate them acoustically from other types of object in the sea.

The results of this research have been presented at: (a) The 177th Meeting of the Acoustical Society of America in Louisville, Kentucky 13-17 May 2019 [9]. (b) The 179th Meeting of the Acoustical Society of America "*Acoustics Virtually Everywhere*," 7-11 December 2020 [10].

REFERENCES

(1) C. Feuillade, R.W. Nero and R. H. Love, " A low frequency acoustic scattering model for small schools of fish," J. Acoust. Soc. Am., **99**, 196-208 (1996).
(2) R. H. Love, " Resonant acoustic scattering by swim bladder-bearing fish," J. Acoust. Soc. Am. **64**, 571-580 (1978).
(3). S. E. Alfaro, J. A. Cellio, M. P. Raveau and C. Feuillade, "Low frequency scattering from dynamic fish schools based on collective animal behavior modeling," Proceedings of Meetings on Acoustics Vol. 23, (2015), DOI: http://dx.doi.org/10.1121/2.0000090
(4) I. D. Couzin, J. Krause, R. James, G. D. Ruxton and R. N. Franks, " Collective memory and spatial sorting in animal groups," J. Theor. Biol., **216**, 1-11 (2002).
(5) J. Krause and G.D. Ruxton, *Living in Groups*, Oxford University Press, (2002).
(6) P.C. Waterman, "New formulation of acoustic scattering," J. Acoust. Soc. Am., **45**, 1417-1429 (1969).
(7) C. Feuillade, "Superspheroidal modeling of resonance scattering from elongated air bubbles and fish swim bladders," J. Acoust. Soc. Am. **131**(1), 146-155 (2012).
(8) M. Raveau and C. Feuillade, "Resonance scattering by fish schools: A comparison of two models," J. Acoust. Soc. Am., **139**, 163-175 (2016).
(9) L. Donoso and C. Feuillade, " Low frequency acoustical scattering from dynamic schools of swim bladder fish," J. Acoust. Soc. Am., **145**, 1654 (2019).
(10) L. Donoso and C. Feuillade, "Geometrical modeling and analysis of low frequency acoustical scattering from cylindrically formed schools of swim bladder fish," J. Acoust. Soc. Am., **148**, 2482 (2020).